Control Engineering Practice 169 (2026) 106768

Contents lists available at ScienceDirect

Control Engineering Practice

journal homepage: www.elsevier.com/locate/conengprac

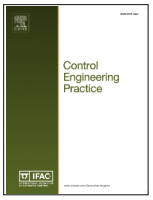

Robust control design to prevent unsteady bulging in continuous slab casters

Julian Landauer [a,*], Paul Dollhäubl [b], Stefan Fuchshumer [b], Wilhelm Posch [b], Andreas Kugi [c], Andreas Steinboeck [a]

[a] Christian Doppler Laboratory for Intelligent Process Control for High-Quality Steel Products, Automation and Control Institute, TU Wien, Vienna, Austria
[b] voestalpine Stahl GmbH, Linz, Austria
[c] Automation and Control Institute, TU Wien, Vienna, Austria

ARTICLE INFO

Keywords:
Continuous casting
Steel slab
Mold level
Unsteady bulging
Robust control
Gain scheduling
Adaptive control
Model-based controller design

ABSTRACT

In continuous casting of steel slabs, the ferrostatic pressure in the liquid core of the strand causes bending (also called bulging) of the strand shell between the guiding rolls. Unsteady bulging refers to a time-varying bending of the strand shell, leading to unwanted mold level fluctuations that can degrade the quality of the cast strand. Most mold level controller designs presented in the literature do not explicitly account for this disturbance due to the absence of suitable unsteady bulging models. As a result, these controllers often fail to sufficiently suppress unsteady bulging or even provoke it. This work presents a novel robust model-based controller design that systematically considers unsteady bulging by incorporating a control-oriented unsteady bulging model. Unlike previous approaches, the proposed method also accounts for variations in plant parameters to ensure robust suppression of unsteady bulging and consistent control performance across the entire range of operating conditions. The proposed controller is validated on industrial continuous slab casters, where it is now permanently used and achieves a significant reduction in mold level fluctuations.

1. Introduction

In a continuous caster, liquid steel is cast into semi-finished products like slabs. The upper section of a continuous slab caster is shown in Fig. 1.

Liquid steel flows from a tundish through a submerged entry nozzle (SEN) into a water-cooled copper mold with rectangular cross-section (area $A = HW$). Inside the mold, also known as the primary cooling zone, the steel begins to solidify from the outer surface, forming a solid strand shell, i.e., a rectangular tube. Below the mold, the strand shell is supported by an array of rolls (on the wide face), which also transport the strand with casting speed v. Water sprays further cool the strand in this region, referred to as the secondary cooling zone. The rolls are grouped into segments numbered by n. Within segment n, the individual roll distances l_k, where k denotes the roll number, are equal to (or non-uniformly distributed about) the specific roll pitch L_n (Murakami et al., 2004). The ferrostatic pressure p in the liquid core of the strand leads to the bending deflection b, so-called bulging, of the wide-face shell between the supporting rolls, see Fig. 1.

The mold level y_m represents the spatially averaged height of the liquid steel surface (meniscus) in the mold. This surface is covered by a slag layer, which protects it from exposure to ambient air and thus oxidation. Furthermore, liquid slag is drawn into the narrow gap between the strand shell and the mold wall, where it functions both as a lubricant and for regulating heat transfer (Craig et al., 2001). Maintaining a flat and constant liquid steel surface is essential for consistent process conditions, uniform (initial) growth of the strand shell, and thus for producing high-quality slabs. Fluctuations of the mean mold level occur if the inflow q of steel through the SEN is unequal to the outflow from the mold, see Fig. 1. Such fluctuations can lead to a non-uniform initial shell growth or entrapment of particles from the slag layer into the strand, thereby compromising product quality (Cukierski & Thomas, 2008; Zhang et al., 2020). Slabs affected by surface defects typically require postprocessing, such as scarfing (Lee et al., 2024), which is both time-consuming and cost-intensive.

Therefore, feedback control is essential to keep the mold level at its constant set point and to reject disturbances. To this end, the mold level is measured, e.g., by electromagnetic field sensors (eddy-current sensors) (Saleem et al., 2020). The steel inflow q into the mold is

* Corresponding author.
E-mail addresses: landauer@acin.tuwien.ac.at (J. Landauer), paul.dollhaeubl@voestalpine.com (P. Dollhäubl), stefan.fuchshumer@voestalpine.com (S. Fuchshumer), wilhelm.posch@voestalpine.com (W. Posch), kugi@acin.tuwien.ac.at (A. Kugi), steinboeck@acin.tuwien.ac.at (A. Steinboeck).

https://doi.org/10.1016/j.conengprac.2026.106768
Received 18 September 2025; Received in revised form 12 December 2025; Accepted 5 January 2026
Available online 15 January 2026

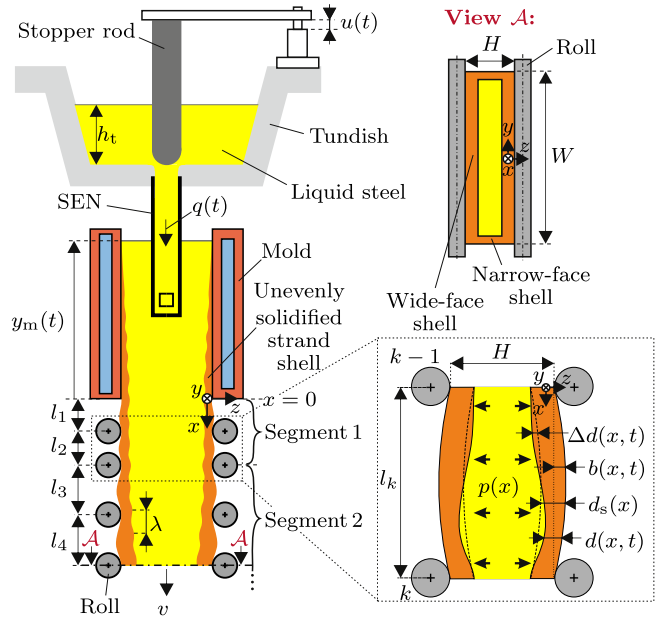

Fig. 1. Upper section of a continuous slab caster with a detailed view of bulging of the strand shell between the rolls.

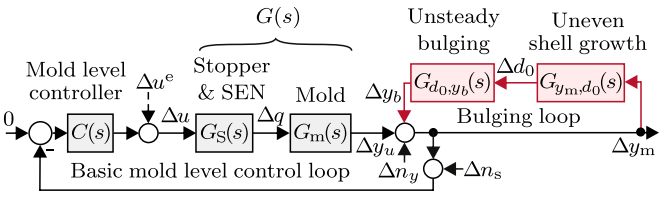

Fig. 2. Transfer function model of the overall mold level control loop, including the basic mold level control loop (black) and the bulging loop (red), for constant casting speed ($\Delta v = 0$).

controlled by a valve equipped with a vertically actuated stopper rod, where u denotes its position, cf. Fig. 1. This results in the basic mold level control loop shown in Fig. 2 in black.

Unwanted variations in the steel inflow q and resulting mold level fluctuations can be caused by turbulent flow patterns in the SEN (Tacke, 2014), clogging, which is the accumulation of aluminum oxide on the stopper rod or inside the SEN, or unclogging, where deposits are partially dislodged. In industrial practice, clogging and unclogging are mitigated by injecting argon gas into the submerged entry nozzle (SEN) at the tip of the stopper rod (Bai & Thomas, 2001), and both the SEN and the stopper rod are regularly replaced. The steel outflow can be disturbed, e.g., by (fast) changes of the casting speed or unsteady bulging. Unsteady bulging refers to a time-varying bending deflection b of the strand shell between the rolls in the secondary cooling zone (see Fig. 1), which induces periodic changes in the volume enclosed by the strand shell. This results in periodic variations in the steel outflow and mold level fluctuations. Figure 3 presents the amplitude spectrum of measured mold level fluctuations caused by unsteady bulging.

This amplitude spectrum indicates harmonic oscillations (approximately) at the so-called bulging frequencies

$$f_{i,n} = i\frac{v}{L_n} \quad i, n \in \mathbb{N}, \tag{1}$$

where v is the casting speed and L_n is the roll pitch in segment n. These frequencies correspond to integer multiples of the frequency $\frac{v}{L_n}$ with which a point on the strand passes support rolls of segment n. At the frequencies $f_{i,n}$ according to (1), the individual time-varying bending deflections between the rolls of segment n are synchronous, i.e., in phase.

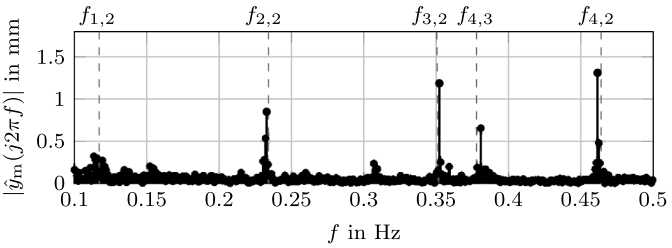

Fig. 3. Typical amplitude spectrum of the mold level disturbed by unsteady bulging measured on a continuous slab caster.

The individual effects of synchronous variations in the bending deflections on the mold level sum up and can thus cause high mold level fluctuations, cf. (Landauer et al., 2024). In contrast, the individual effects of non-synchronous variations in the bending deflections on the mold level (partially) cancel each other out and are thus not critical. At the considered industrial slab caster, measurable mold level fluctuations caused by unsteady bulging are observed at frequencies associated with the segments $n = 1$ to 8 and up to the multiple $i = 7$.

Lee and Yim (2000) showed that unsteady bulging can result from variations Δd of the thickness of the strand shell (with wavelength λ), as indicated in Fig. 1. Such thickness variations stem from an uneven solidification of the strand shell, which can be caused by mold level fluctuations, cf. (Azizi et al., 2020). These mold level fluctuations, in turn, may result from unsteady bulging, which creates an internal feedback loop, the so-called bulging loop (Furtmueller & del Re, 2008; Hirschmanner et al., 2011; Lamant et al., 1990; Landauer et al., 2024; Yoon et al., 2002). This loop is shown in Fig. 2 in red. Landauer et al. (2024) presented a control-oriented model of the bulging loop. They showed that the emergence of unsteady bulging with continuously growing amplitudes, so-called self-excited unsteady bulging, is related to an unstable overall mold level control loop, which is the combination of the basic mold level control loop and the bulging loop, see Fig. 2. The control behavior of the basic mold level control loop plays a significant role in the emergence and behavior of unsteady bulging. This will be discussed in more detail in Section 2.3.

Typically, PI/PID control (Kong & de Keyser, 1993; Lamant et al., 1990), lead-lag compensation (Kong & de Keyser, 1993), fuzzy control (Feng et al., 2020; González-Yero et al., 2021; Zhang & Ji, 2014), iterative learning control (You et al., 2011), model predictive control (De Keyser, 1997), H_∞-control (Iijima & Mizuno, 2007; Kitada et al., 1998; Kurokawa et al., 1993; Schuurmans et al., 2005), and adaptive control (González-Yero et al., 2018; Jabri et al., 2010) are used to feedback control the mold level. In the design of these controllers, the internal feedback loop associated with unsteady bulging is typically ignored. As a result, the control action often fails to sufficiently suppress unsteady bulging or may even provoke it. Therefore, disturbance-feedforward concepts are often used in addition to the basic mold level controller to selectively suppress identified mold level disturbances caused by unsteady bulging, see, e.g., (Furtmueller et al., 2012; Jabri et al., 2008, 2011; Kim et al., 2011). In this case, unsteady bulging is considered as an unknown exogenous harmonic disturbance. Its frequency, amplitude, and phase are estimated by an observer. Tests on the considered industrial slab caster showed that even small estimation errors can significantly degrade the performance of this disturbance-feedforward control approach. Reliable estimation requires a low model-plant mismatch of the observer model and sufficiently long measurements (depending on the signal-to-noise ratio), which introduces an additional delay in the control loop and limits the control bandwidth.

Failure of a control concept means that the amplitudes of unsteady bulging continuously increase, which can cause serious defects in the cast strand or, in the worst case, a breakout of the strand shell. A common strategy to prevent this situation is to reduce the casting speed. This measure suppresses unsteady bulging by increasing the strand shell

thickness, as discussed in (Landauer et al., 2024). However, the drawback of this strategy includes reduced plant throughput and additional costs. In contrast, employing a suitable mold level controller that effectively suppresses unsteady bulging by rejecting the associated mold level fluctuations, thereby fostering uniform growth of the strand shell, is a more efficient solution. Based on this solution idea, the present paper introduces a novel robust controller design. Unlike previous approaches presented in the literature, this design systematically incorporates the bulging loop. To this end, a control-oriented model of the bulging loop presented in (Landauer et al., 2024) is utilized.

1.1. Related work

There are a few works like (Iijima & Mizuno, 2007), where H_∞-synthesis is used to design a controller with increased control action in the typical frequency range of mold level fluctuations caused by unsteady bulging. However, Iijima and Mizuno (2007) did not systematically consider the dynamic behavior of unsteady bulging by means of a model of the bulging loop and tested their solution only in simulations. The analysis conducted in Section 2.1 of the present paper reveals high (temporal) variations in the plant parameters. Such variations should be considered in the design of a mold level controller to ensure robust stability and sufficient control performance across the entire range of plant parameter values. González-Yero et al. (2018) account for these variations by means of a gain-scheduled PI controller. However, they did not account for the bulging loop or variations in the dead time of the plant.

1.2. Contribution of this work

This work presents a novel, robust mold level controller design, specifically aimed at suppressing unsteady bulging. Unlike existing mold level controller designs in the literature, the internal feedback mechanism associated with unsteady bulging is systematically considered in the controller design by incorporating a control-oriented unsteady bulging model. The outcome is a novel gain-scheduled controller that dynamically adapts its parameters in response to variations in the plant parameters. To support this adaptability, a method for online estimation of the relevant plant parameters is also introduced.

1.3. Outline of this work

A model of the overall mold level control loop, including the basic mold level control loop and the bulging loop, is presented in Section 2. Furthermore, this section summarizes key insights from (Landauer et al., 2024) relevant for the design of a mold level controller to systematically suppress unsteady bulging. Section 3 presents the design of two robust controllers, which can suppress unsteady bulging. The first controller has fixed parameters. The second controller incorporates gain scheduling to account for variations in the plant parameters. While both controllers effectively suppress unsteady bulging, the gain-scheduled controller achieves notably better control performance. Section 4 presents the validation of the developed gain-scheduled controller and shows a significant reduction of mold level fluctuations associated with unsteady bulging. Finally, Section 5 presents some concluding remarks.

2. Model of the overall mold level control loop

This section recaps the transfer-function model of the overall mold level control loop presented in (Landauer et al., 2024). This model describes the plant behavior in terms of small deviations (denoted as Δ) from the steady state. Additionally, this section summarizes key insights relevant to the systematic design of a controller for suppressing unsteady bulging. The overall mold level control loop consists of the basic mold level control loop and the bulging loop, shown in black and red, respectively, in Fig. 2.

2.1. Basic mold level control loop

The transfer function[1] describing how changes of the stopper rod position Δu influence fluctuations in the inflow rate Δq of liquid steel into the mold is typically considered in the form (Furtmueller & del Re, 2008; González-Yero et al., 2018; Jabri et al., 2011; Kim et al., 2011; Lamant et al., 1990)

$$G_\mathrm{S}(s) = \frac{\Delta\hat{q}(s)}{\Delta\hat{u}(s)} = \sqrt{\frac{h_\mathrm{t}}{h_\mathrm{t}^0}}\, V_\mathrm{S} \exp(-s\tau_\mathrm{S}). \tag{2}$$

Here, V_S denotes the gain and τ_S the dead time between a movement of the stopper rod and the reaction of the mold level. This dead time can significantly influence the achievable control performance of the basic mold level control loop (Asano et al., 1996; Jabri, 2010). The term $\sqrt{h_\mathrm{t}/h_\mathrm{t}^0}$ accounts for the dependence of the steel flow q through the SEN on the steel level h_t in the tundish relative to the nominal level h_t^0, see Fig. 1. The position $u(t)$ of the stopper rod is feedback controlled by a hydraulic system that uses a separate (cascade) controller whose bandwidth exceeds that of the basic mold level control loop by more than an order of magnitude. Consequently, the actuator dynamics are approximated by the transfer function 1 within the considered frequency range.

The relationship between changes in the steel inflow Δq and resulting fluctuations in the mean mold level Δy_u can be expressed through the transfer function

$$G_\mathrm{m}(s) = \frac{\Delta\hat{y}_u(s)}{\Delta\hat{q}(s)} = \frac{1}{sA} \tag{3}$$

derived from a volume balance, where $A = HW$ denotes the mold area, see Fig. 1. The transfer function, relating changes in the stopper rod position Δu to resulting mold level fluctuations Δy_u, is given by the product of (2) and (3)

$$G(s) = G_\mathrm{S}(s)G_\mathrm{m}(s) = \sqrt{\frac{h_\mathrm{t}}{h_\mathrm{t}^0}}\frac{V_\mathrm{S}}{sA}\exp(-s\tau_\mathrm{S}). \tag{4}$$

The dynamics of the mold level sensors used at the considered industrial caster exceed the control bandwidth of the basic mold level control loop by more than an order of magnitude. Consequently, within the considered frequency range, the sensor is approximated by the transfer function 1 and additive sensor noise Δn_s (see Fig. 2).

During normal operation, the casting speed v is typically constant or it changes slowly enough to be considered quasi-constant, i.e., $\Delta v = 0$. Significant (temporal) variations in the plant parameters V_S and τ_S can be observed during casting. These variations are mainly caused by clogging or wear of the stopper rod and the SEN and changing casting conditions (Asano et al., 1996; Furtmueller et al., 2012; Jabri, 2010; Lamant et al., 1990). To explore variations in the plant parameters in detail, dedicated measurements were conducted at an industrial plant. The mold level was excited by harmonic oscillations Δu^e applied to the stopper rod, cf. Fig. 2, with frequency f_e and amplitudes that do not compromise the product quality. The frequency response of $G(s)$ can then be estimated (pointwise) according to

$$G^\mathrm{e}(j2\pi f_\mathrm{e}) = \frac{\Delta\hat{y}_\mathrm{m}(j2\pi f_\mathrm{e})}{\Delta\hat{u}(j2\pi f_\mathrm{e})}, \tag{5}$$

where $\Delta\hat{y}_\mathrm{m}(j2\pi f_\mathrm{e})$ and $\Delta\hat{u}(j2\pi f_\mathrm{e})$ correspond to the frequency components of the measured mold level Δy_m and the stopper rod position Δu, respectively, at the frequency f_e. Comparing (4) and (5) gives the estimated plant parameters

$$V_\mathrm{S}^\mathrm{e} = 2\pi f_\mathrm{e} A\sqrt{\frac{h_\mathrm{t}^0}{h_\mathrm{t}}}\left|G^\mathrm{e}(j2\pi f_\mathrm{e})\right|, \quad \tau_\mathrm{S}^\mathrm{e} = -\frac{1}{2\pi f_\mathrm{e}}\left(\arg(G^\mathrm{e}(j2\pi f_\mathrm{e})) + \frac{\pi}{2}\right). \tag{6}$$

[1] Henceforth, a hat on a symbol refers to the corresponding Laplace-transformed quantity.

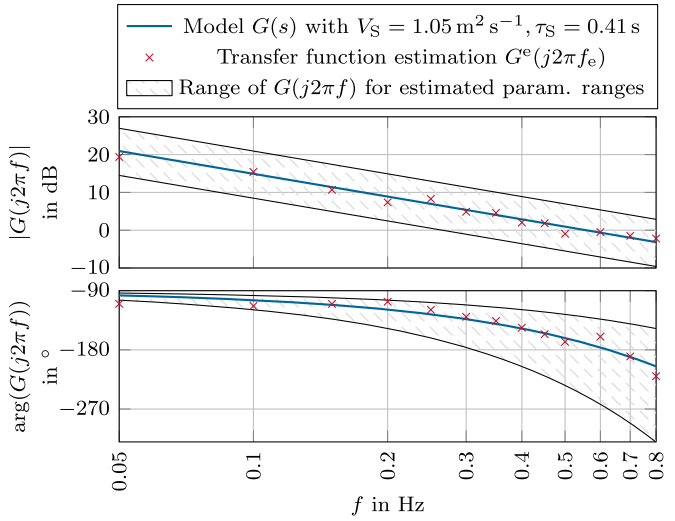

Fig. 4. Comparison of the frequency response of the model $G(s)$ defined in (4) with measurements $G^e(j2\pi f_e)$ according to (5).

For a typical operating scenario, Fig. 4 compares the obtained measurement results and the model $G(s)$ with identified parameter values. This corroborates that the structure of the model $G(s)$ according to (4) is appropriate for describing the measured dynamic behavior of the plant within the shown frequency range.

Repeating this identification for other operating scenarios and other conditions (clogging, wear) of the stopper rod and the SEN revealed that the estimated parameters can vary within the ranges

$$V_S^e \in [0.5, 2.1]\,\mathrm{m^2/s}, \quad \tau_S^e \in [0.2, 0.8]\,\mathrm{s}. \tag{7}$$

The corresponding uncertainty of $G(s)$ is indicated by the gray hatched area in Fig. 4.

In the continuous caster considered for this work, a manually tuned PI controller with the transfer function

$$C_{PI}(s) = \underbrace{A\sqrt{\frac{h_t^0}{h_t}}}_{K}\underbrace{\left(K_p + \frac{K_i}{s}\right)}_{C_{PI}^0(s)} \tag{8}$$

has been used so far, with parameter values of $K_p = 0.81\,\mathrm{m^{-2}}$ and $K_i = 0.0541\,\mathrm{m^{-2}s^{-1}}$. The mold area A and the steel level h_t in the tundish are accurately known parameters that vary only slowly over time. With the choice of the gain K in (8), the parameters A, h_t, and h_t^0 cancel out in the open-loop transfer function $G(s)C(s)$ for $C(s) = C_{PI}(s)$, cf. (4), and therefore do not influence the control performance (in terms of rejection of output disturbances).

The control performance of the basic mold level control loop, cf. Fig. 2, is characterized by the transfer functions

$$S(s) = \frac{1}{1 + G(s)C(s)}, \tag{9a}$$

$$T(s) = 1 - S(s) = \frac{G(s)C(s)}{1 + G(s)C(s)}, \tag{9b}$$

$$C(s)S(s) = \frac{C(s)}{1 + G(s)C(s)}. \tag{9c}$$

$S(s)$ and $T(s)$ are the sensitivity function and the complementary sensitivity function, respectively. The sensitivity function quantifies the effectiveness of the mold level controller in rejecting output disturbances Δn_y, i.e., it describes the transfer characteristic from output disturbances Δn_y to resulting mold level fluctuations Δy_m, cf. Fig. 2. The complementary sensitivity function characterizes, among other things, the influence of sensor noise Δn_s (see Fig. 2) on the mold level. The product $C(s)S(s)$ describes the response of the stopper rod position Δu to output disturbances Δn_y. These transfer functions will be employed in Section 3 to facilitate a systematic controller design.

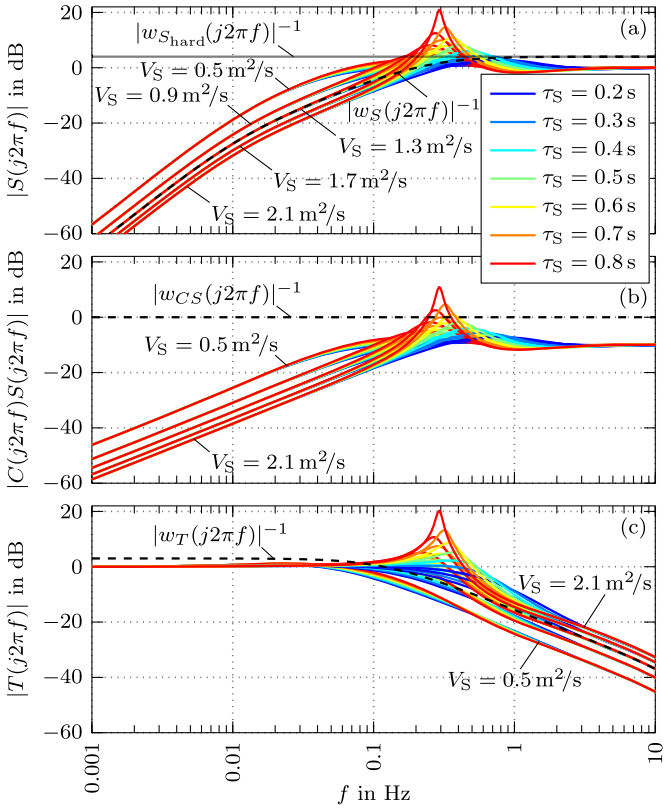

Fig. 5. Frequency responses of $S(s)$, $C(s)S(s)$, and $T(s)$ according to (9) for the PI controller $C(s) = C_{PI}(s)$ defined in (8) and different values of the plant parameters V_S and τ_S.

Figure 5 shows the corresponding frequency responses of $S(s)$, $C(s)S(s)$, and $T(s)$ for different values of the plant parameters V_S and τ_S within the identified ranges according to (7) and the PI controller $C(s) = C_{PI}(s)$ defined in (8).

From standard control theory, see, e.g., (Skogestad & Postlethwaite, 2005), it is known that these frequency responses can be separated into three frequency regions based on the frequency response $|G(j2\pi f)C(j2\pi f)|$ of the open basic mold level control loop, which is shown in Fig. 6. The following relations, which can be inferred from (9), hold true:

1. $|S(j2\pi f)| \approx 1/|G(j2\pi f)C(j2\pi f)|$ and $|T(j2\pi f)| \approx 1$ at low frequencies f where $|G(j2\pi f)C(j2\pi f)| \gg 1$.
2. $|S(j2\pi f)| \approx 1$ and $|T(j2\pi f)| \approx |G(j2\pi f)C(j2\pi f)|$ at high frequencies f where $|G(j2\pi f)C(j2\pi f)| \ll 1$.

Thus, at both low and high frequencies, $|S(j2\pi f)|$ and $|T(j2\pi f)|$ are approximately independent of the dead time τ_S, which may also be inferred from Fig. 5. However, in the intermediate frequency region where $|G(j2\pi f)C(j2\pi f)| \approx 1$, both $|S(j2\pi f)|$ and $|T(j2\pi f)|$ depend significantly on the dead time τ_S, cf. (9) and Fig. 5.

The control bandwidth, defined as the frequency where $|S(j2\pi f)|$ first exceeds -3 dB (Skogestad & Postlethwaite, 2005), is strongly influenced by the plant gain V_S, as shown in Fig. 5(a). Within the control bandwidth, output disturbances Δn_y, see Fig. 2, are effectively attenuated by the basic mold level control loop. However, due to the so-called waterbed effect (Skogestad & Postlethwaite, 2005), the magnitude of the sensitivity function $|S(j2\pi f)|$ inevitably exceeds 0 dB at frequencies beyond the control bandwidth, leading to a pronounced peak, commonly referred to as the sensitivity peak. At these frequencies, disturbances are

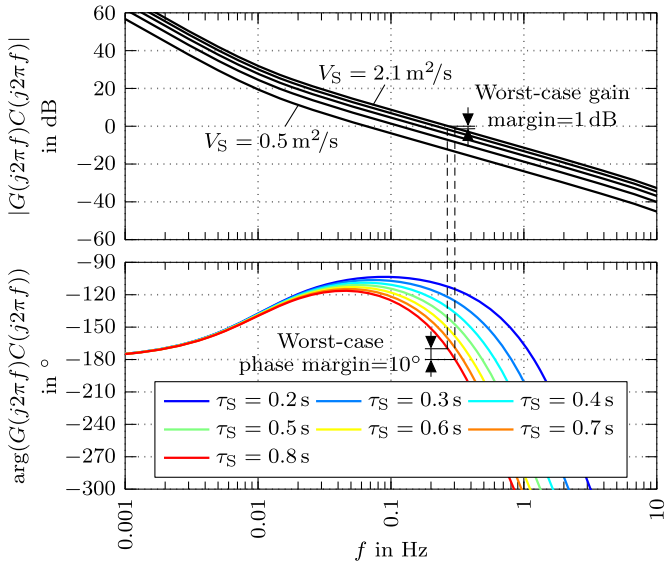

Fig. 6. Frequency response of the open basic mold level control loop $G(s)C(s)$, cf. Fig. 2, for the PI controller $C(s) = C_{\mathrm{PI}}(s)$ defined in (8) and different values of the plant parameters V_S and τ_S. The magnitude does not depend on the dead time τ_S and is therefore shown in black.

amplified by the basic mold level control loop. The height of the sensitivity peak depends on the plant parameters V_S and τ_S, which, in turn, depend on the casting conditions and the condition (clogging, wear) of the stopper rod and the SEN. The sensitivity peaks shown in Fig. 5(a) are especially high for large values of V_S and τ_S. According to Skogestad and Postlethwaite (2005), high sensitivity peaks are associated with low phase and gain margins of the control loop, as illustrated in Fig. 6. Consequently, a controller design that increases both the phase and the gain margin also reduces the height of the sensitivity peaks.

As demonstrated in the following section, high sensitivity peaks not only amplify disturbances in the related frequency range but can also destabilize the overall mold level control loop (see Fig. 2), leading to unsteady bulging. To avoid this, Section 3 presents a robust controller design that minimizes these sensitivity peaks across the entire range of plant parameter values (7) and, consequently, facilitates an effective way to suppress unsteady bulging in continuous slab casters.

2.2. Bulging loop

Figure 2 indicates that the bulging loop consists of two sub-models $G_{y_m,d_0}(s)$ and $G_{d_0,y_b}(s)$, capturing an uneven growth of the strand shell in the mold (see Fig. 1) and the resulting unsteady bulging of the strand shell between the supporting rolls, respectively. As described in (Landauer et al., 2024), the local thickness variation $\Delta d(x,t)$ of the strand shell in the roll array ($x > 0$) originates from uneven (initial) solidification in the mold, caused by mold level fluctuations. The local thickness variations $\Delta d(x,t)$ are determined by the (harmonic) thickness variation $\Delta d_0(t) = D\sin(2\pi f t)$ leaving the mold at the mold exit ($x = 0$). It is assumed that this thickness variation approximately persists as it moves downward through the roll array with the strand at the casting speed v, which can be expressed as

$$\Delta d(x,t) = \Delta d_0\left(t - \frac{x}{v}\right), \quad x \geq 0. \tag{10}$$

The uneven growth of the strand shell in the mold, caused by mold level fluctuations, is formulated by the transfer function

$$G_{y_m,d_0}(s) = \frac{\Delta\hat{d}_0(s)}{\Delta\hat{y}_m(s)} = V_{\mathrm{shell}} \exp\left(-s\frac{y_{m,s}}{v}\right). \tag{11}$$

It relates mold level fluctuations Δy_m and resulting thickness variations Δd_0 at $x = 0$. V_{shell} represents the sensitivity of the (initial) shell growth to mold level fluctuations and is especially high for peritectic steel grades, cf. (Azizi et al., 2020; Lei et al., 2023; Xia et al., 2011). The time delay $\frac{y_{m,s}}{v}$ represents the transport time of the strand shell through the mold, where the transport distance is the steady-state mold level $y_{m,s}$.

A control-oriented unsteady bulging model that captures the relationship between thickness variations Δd_0 and mold level fluctuations Δy_b caused by unsteady bulging (see Fig. 2) was first developed by Landauer et al. (2024). This model is suitable for stability analysis in closed-loop simulations and for systematic control design and tuning using frequency-domain methods. It is based on a detailed bulging model derived from beam bending theory. In this model, the solid strand shell is treated as a beam with a local thickness $d(x,t)$ and a time-invariant temperature distribution $T(x,z)$. These properties are assumed to be identical for both wide faces of the strand and independent of the transverse direction y (see Fig. 1). The strand shell is supported by rolls and bulges between these rolls because of the ferrostatic pressure

$$p(x) = \rho g h(x), \tag{12}$$

as illustrated in Fig. 1. Here, ρ, g, and h represent the liquid steel density, the gravitational acceleration, and the vertical distance between the mold level and the cross-section of the strand at the position x, respectively. The model captures elastic and viscoplastic (creep) deformation. The high temperature of the strand shell promotes viscoplastic deformation, which significantly contributes to the overall bulging deflections. A nonlinear bulging model is derived in (Landauer et al., 2024) by applying constitutive equations (including a nonlinear creep law) and material parameters from (Kozlowski et al., 1992) together with basic beam bending theory. This model accurately captures the bending deflection b (see Fig. 1) and the bending moment M, which are governed by the boundary value problem

$$\frac{\partial^2 b(x,t)}{\partial x^2} = \kappa(x,t), \tag{13a}$$

$$\frac{\partial^2 M(x,t)}{\partial x^2} = -W p(x), \tag{13b}$$

with the boundary conditions

$$\frac{\partial b}{\partial x}(0,t) = 0, \quad \frac{\partial b}{\partial x}(x_N,t) = 0, \tag{14a}$$

$$b(x_k,t) = 0 \quad \forall k = 0,1,\ldots,N, \tag{14b}$$

where x_k denotes the position of roll number k. The curvature κ is the sum of an elastic component

$$\kappa_e(x,t) = -\frac{M(x,t)}{\xi(x,d)}, \tag{15}$$

where ξ denotes the bending stiffness, and a viscoplastic component κ_c, governed by the nonlinear differential equation (inhomogeneous transport equation)

$$\frac{\partial \kappa_c(x,t)}{\partial t} + v\frac{\partial \kappa_c(x,t)}{\partial x} = \dot{\kappa}_c(x,t) = \\ -\frac{M(x,t) - M_h(x,\kappa_c,d)}{I_c(x,d)^{c(\bar{T}(x))}} |M(x,t) - M_h(x,\kappa_c,d)|^{c(\bar{T}(x))-1}. \tag{16}$$

$\bar{T}$ is the local mean temperature of the strand shell averaged over z, see Fig. 1, and c is known as the creep exponent. The term I_c represents the so-called creep integral (Lamant et al., 1985) and can be understood as the resistance of the beam against viscoplastic bending deformation. In (16), M_h represents an opposing bending moment that accounts for hardening effects. A more detailed explanation of the terms in (16) is given in (Landauer et al., 2024).

The nonlinear bulging model (12)–(16) describes the entire dynamic behavior of bulging, including the steady state denoted by the subscript s. However, the computational complexity of this nonlinear model

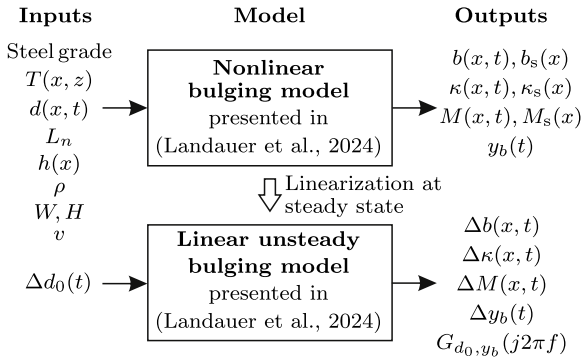

Fig. 7. Overview of considered bulging models.

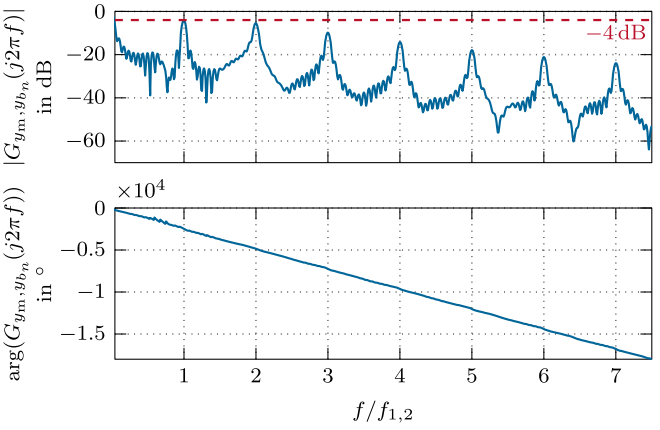

Fig. 8. Frequency response $G_{y_m,y_{b_n}}(j2\pi f)$ of the (open) bulging loop in Fig. 2, for segment $n = 2$ with roll pitch $L_2 = 185$ mm and a casting speed of $v = 1.3$ m/min.

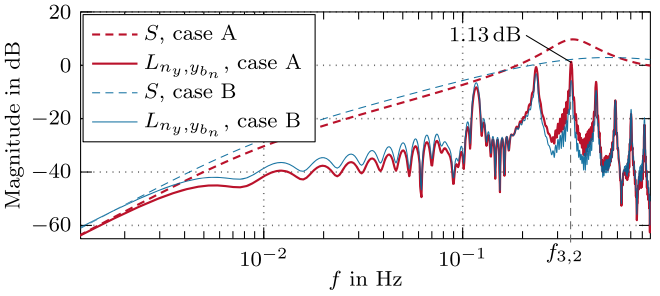

Fig. 9. Frequency responses of the sensitivity function $S(s)$ (of the basic mold level control loop) and the open-loop transfer function $L_{n_y,y_{b_n}}(s)$ for segment $n = 2$. Case A with the parameter values $V_S = 1.8\,\mathrm{m^2\,s^{-1}}$, $\tau_S = 0.57$ s and case B with the parameter values $V_S = 1.5\,\mathrm{m^2\,s^{-1}}$, $\tau_S = 0.3$ s. $V_{\mathrm{shell}} = 1.45$ holds true in both cases.

makes it unsuitable for analyzing dynamic system behavior in the frequency domain or in closed-loop simulations, which is essential for a systematic controller design. Therefore, the model is simplified through linearization around the steady state. This linearization step is acceptable because unsteady bulging corresponds to small deviations from the steady state. Figure 7 provides a graphical overview of the bulging models and summarizes the related inputs and outputs. By applying the Laplace transformation to the linearized model, the transfer function

$$G_{d_0,y_{b_n}}(s) = \frac{\Delta\hat{y}_{b_n}(s)}{\Delta\hat{d}_0(s)} \tag{17}$$

describing unsteady bulging is obtained. In fact, (17) describes mold level fluctuations Δy_{b_n} associated with unsteady bulging in segment n caused by thickness variations Δd_0 of the strand shell. The contributions Δy_{b_n} from the individual segments superpose and form the overall mold level fluctuations Δy_b due to bulging. Although the linear unsteady bulging model from (Landauer et al., 2024) does not yield an analytical expression for (17), it can be numerically evaluated with $s = j2\pi f$ for specific frequencies f, to obtain the frequency response $G_{d_0,y_{b_n}}(j2\pi f)$ (pointwise).

The product of (11) and (17) then gives the transfer function

$$G_{y_m,y_{b_n}}(s) = G_{d_0,y_{b_n}}(s)G_{y_m,d_0}(s) \tag{18}$$

of the (open) bulging loop, cf. Fig. 2, describing the relation between the total mold level fluctuations Δy_m and mold level fluctuations Δy_{b_n} due to resulting unsteady bulging for the individual segments numbered by n. Figure 8 shows the corresponding frequency response $G_{y_m,y_{b_n}}(j2\pi f)$ for segment $n = 2$ with roll pitch $L_2 = 185$ mm and a casting speed of $v = 1.3$ m/min (a detailed list of the operating conditions can be found in (Landauer et al., 2024)).

The frequency f is normalized with respect to the first harmonic $f_{1,2}$ of the bulging frequencies of segment 2, see (1). Significant peaks are observed at the frequencies $f_{i,2} = i f_{1,2}, i \in \mathbb{N}$. At these frequencies, an integer multiple i of the wavelength λ of the thickness variation Δd, cf. Fig. 1, matches the roll pitch in segment 2, causing synchronous oscillations of the strand shell between the rolls of this segment, see (Landauer et al., 2024). The heights of these peaks asymptotically decrease by 40 dB/dec. The high phase values result from the transport time of the strand shell from the mold level to the respective rolls.

2.3. Stability analysis of the overall mold level control loop

BIBO (Bounded-Input, Bounded-Output) stability of the (closed) overall mold level control loop can be evaluated using the transfer function

$$L_{n_y,y_{b_n}}(s) = \frac{\Delta\hat{y}_{b_n}(s)}{\Delta\hat{n}_y(s)} = G_{y_m,y_{b_n}}(s)S(s). \tag{19}$$

It describes the relation between output disturbances Δn_y and mold level fluctuations Δy_{b_n} caused by unsteady bulging in segment n, considering an open bulging loop and a closed basic mold level control loop, cf. Fig. 2. According to (Landauer et al., 2024), the closed overall mold level control loop is potentially unstable if[2] the open-loop gain $|L_{n_y,y_{b_n}}(j2\pi f)|$ exceeds 0 dB for any segment n and at any frequency f.

Figure 9 shows the open-loop gain $|L_{n_y,y_{b_n}}(j2\pi f)|$ for segment $n = 2$ together with the sensitivity function $|S(j2\pi f)|$ of the basic mold level control loop for two different sets of parameter values (case A and B). Both (19) and Fig. 9 show that the height of the individual peaks in $|L_{n_y,y_{b_n}}(j2\pi f)|$ depends on $|S(j2\pi f)|$. Active damping by the basic mold level control loop ($|S(j2\pi f)| < 1$) is achieved only for the first peak in $|L_{n_y,y_{b_n}}(j2\pi f)|$ at $f_{1,2} = 0.117$ Hz. The remaining peaks in $|L_{n_y,y_{b_n}}(j2\pi f)|$ are located beyond the control bandwidth of the basic mold level control loop and are actually amplified, particularly within the frequency range surrounding the sensitivity peak.

The location and height of this sensitivity peak, in turn, are influenced by the plant parameters V_S and τ_S, as indicated in Fig. 5(a). For the parameter set of case A, the peak in $|L_{n_y,y_{b_n}}(j2\pi f)|$ at the frequency $f_{3,2} = 0.351$ Hz exceeds the 0 dB-line. As a consequence, self-excited unsteady bulging with growing amplitudes was observed near this frequency, as reported in (Landauer et al., 2024). To demonstrate the influence of the location and height of the sensitivity peak on the stability of the overall mold level control loop, Fig. 9 shows $|L_{n_y,y_{b_n}}(j2\pi f)|$ and

[2] A detailed stability analysis based on the Nyquist stability criterion is conducted in (Landauer et al., 2024).

$|S(j2\pi f)|$ also for a second parameter set (case B). For this parameter set, the height of the sensitivity peak is significantly lower. In contrast to case A, none of the peaks in $|L_{n_y,y_{b_n}}(j2\pi f)|$ exceed the 0 dB line in case B, and unsteady bulging did not occur. This indicates that (self-excited) unsteady bulging is linked to an unstable overall mold level control loop.

Based on these insights, it can be concluded that effective strategies for suppressing (self-excited) unsteady bulging should ensure $|L_{n_y,y_{b_n}}(j2\pi f)| < 1$ (0 dB) for all frequencies f and across the entire range of plant parameter values (7). This can be achieved by a reduction of the height of the individual peaks in $|G_{y_m,y_{b_n}}(j2\pi f)|$ or the height of the sensitivity peaks, cf. (19). A reduction of the height of the individual peaks in $|G_{y_m,y_{b_n}}(j2\pi f)|$ can be accomplished by decreasing the casting speed v. This leads to an increase in the thickness of the strand shell and, consequently, reduces the impact of thickness variations on the deflection of the strand shell. The downside of this measure is a reduced plant throughput.

A less intrusive and inexpensive strategy to stabilize the (closed) overall mold level control loop and, consequently, to suppress unsteady bulging is an improved design of the feedback controller to reduce the height of the sensitivity peaks of the basic mold level control loop. This strategy is elaborated in the following section.

3. Robust controller design

The purpose of a robust mold level feedback controller $C(s)$ is to guarantee stability of the overall mold level control loop (see Fig. 2) and to achieve the desired control performance across the entire range of plant parameter values, i.e., robust stability and robust performance. A sufficient (though not necessary) condition for the stability of the overall mold level control loop is that the magnitude $|L_{n_y,y_{b_n}}(j2\pi f)|$, as defined in (19), remains below 1 (0 dB) for any frequency f, all segments n of the roll array, and for the entire range of plant parameter values specified in (7). Figure 8 shows the gain $|G_{y_m,y_{b_n}}(j2\pi f)|$ of the (open) bulging loop for segment $n = 2$. Its highest peak is located at $f_{1,2}$ and has the value −4 dB. At the considered caster, this peak is the highest peak among all segments because segment 2 has the largest number of rolls with equal roll distances, and the strand shell in segment 2 is still relatively thin. Furthermore, the bulging loop gain in Fig. 8 is shown for a peritectic steel grade (see operation conditions in (Landauer et al., 2024)), which causes an extraordinarily high value of V_{shell} in (11). This means that the maximum bulging loop gain of −4 dB shown in Fig. 8 is a worst-case value over all segments and operating conditions. As a consequence, $|L_{n_y,y_{b_n}}(j2\pi f)|$ remains below the 0 dB line if $|S(j2\pi f)|$ does not exceed 4 dB at any frequency f and across the entire range of plant parameter values, as evident from (19) and Fig. 9. Note that this is a conservative criterion because it considers only the magnitude of the highest peak in $|G_{y_m,y_{b_n}}(j2\pi f)|$ of segment 2, whereas other peaks in $|G_{y_m,y_{b_n}}(j2\pi f)|$ would allow for higher sensitivity peak values. However, the criterion $|S(j2\pi f)| < 4$ dB enhances robustness, as the positions $f_{i,n}$ of the peaks in $|G_{y_m,y_{b_n}}(j2\pi f)|$ vary depending on the casting speed v, cf. (1).

A straightforward method to reduce the height of the sensitivity peak, which is also practical to test during industrial operation, is to decrease the overall controller gain. Figure 10 shows the frequency response of the sensitivity function $S(s)$ for the PI controller defined in (8) with overall controller gain reduced to 40 % of its nominal value, i.e., $C(s) = 0.4C_{\text{PI}}(s)$.

A comparison of Fig. 10 with Fig. 5(a) demonstrates that this reduction of the controller gain significantly reduces the height of the sensitivity peaks across the entire range of plant parameter values and ensures that they are below 4 dB, which is expected to be sufficient for suppressing unsteady bulging.

To validate the theoretical insights presented in Section 2.3, a test was conducted on an industrial continuous slab caster at voestalpine Stahl GmbH, in which the controller gain of the PI controller was manually reduced from its nominal value to 40 % during a scenario with unsteady bulging. Figure 11 shows the results of this test.

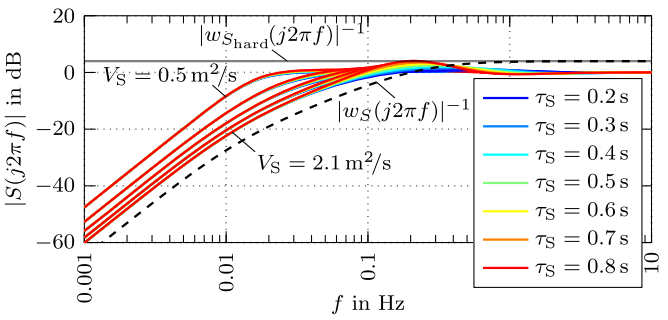

Fig. 10. Frequency response of $S(s)$ according to (9a) for the PI controller defined in (8) with overall controller gain reduced to 40 %, i.e., $C(s) = 0.4C_{\text{PI}}(s)$ and different values of the plant parameters V_S and τ_S.

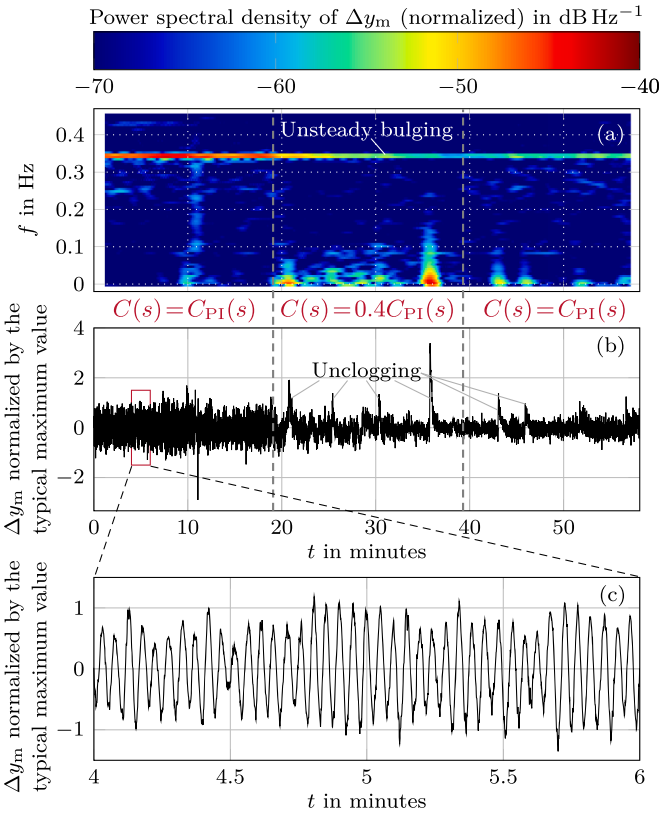

Fig. 11. Changes in the overall controller gain of the PI controller $C(s) = C_{\text{PI}}(s)$ defined in (8) from 100 % to 40 % and back to 100 % of its nominal value during a scenario with unsteady bulging, measured on an industrial slab caster, (a) spectrogram of the mold level fluctuations, (b) mold level fluctuations, (c) mold level fluctuations in a zoomed time interval with high unsteady bulging.

Initially, unsteady bulging resulted in significant harmonic mold level fluctuations at a frequency of approximately 0.34 Hz. Both the mold level signal in Fig. 11(b) and its spectrogram in Fig. 11(a) indicate that mold level fluctuations due to unsteady bulging decrease as soon as the overall controller gain is reduced to 40 % of its nominal value and slowly increase again after setting the overall controller gain back to 100 %. The observed behavior confirms the findings of the conducted stability analysis and practically demonstrates that (self-excited) unsteady bulging can be avoided by a tailored tuning of the mold level controller, even with the basic PI controller (8). However, the reduction of the overall controller gain also leads to a reduced control performance regarding

rejection of (output) disturbances, as the sensitivity function increases within the control bandwidth in Fig. 10 compared to Fig. 5(a). Indeed, the spectrogram in Fig. 11(a) clearly shows an increase in mold level fluctuations for $f < 0.1$ Hz while the overall controller gain was reduced. Some of the peaks in the mold level signal during this time period can be attributed to unclogging events, as marked in Fig. 11(b). In total, this reduced disturbance rejection may lead to increased overall mold level fluctuations, despite the effective suppression of unsteady bulging.

To prevent this undesired reduction in control performance, the controller design should aim to reduce the height of the sensitivity peaks compared to the PI controller, while maintaining comparable values of $|S(j2\pi f)|$ within the control bandwidth. This objective must be achieved across the entire range of plant parameter values. To this end, the design of two robust controllers is presented. The first controller employs fixed parameters, while the second incorporates gain scheduling to adapt to changes in the plant parameters. Although both controllers effectively suppress unsteady bulging, the gain-scheduled controller demonstrates significantly improved control performance compared to its fixed-parameter counterpart.

3.1. Optimized controller with fixed parameters

To achieve this goal, the transfer functions defined in (9) for the basic mold level control loop are systematically shaped while accounting for the full range of plant parameter values. This is accomplished through optimal tuning of a mold level controller described by the transfer function

$$C_m(s) = \underbrace{A\sqrt{\frac{h_\mathrm{t}^0}{h_\mathrm{t}}}}_{K} \underbrace{\frac{b_m s^m + b_{m-1}s^{m-1} + \ldots + b_1 s + b_0}{s^m + a_{m-1}s^{m-1} + \ldots + a_1 s + a_0}}_{C_m^0(s)}, \tag{20}$$

with the known gain K from (8) and the nominal transfer function $C_m^0(s)$ of (fixed) order m. $C_m^0(s)$ is characterized by $2m+1$ tunable parameters, which are assembled in the vector $\mathbf{p} = [a_0, a_1, \ldots, a_{m-1}, b_0, b_1, \ldots, b_m]^\mathrm{T}$ and tuned using the Matlab function `systune`. This function uses the (nonsmooth) optimization algorithms described in (Apkarian et al., 2015, 2014; Apkarian & Noll, 2006, 2007) to optimally tune these parameters in order to guarantee stability and the desired performance of the overall control loop across the entire range of plant parameter values specified in (7). For this purpose, the desired magnitudes of $S(j2\pi f)$, $C(j2\pi f)S(j2\pi f)$, and $T(j2\pi f)$, and thus the target control performance, have to be defined by frequency-dependent weighting functions $|w_\mathrm{S}(j2\pi f)|$, $|w_\mathrm{CS}(j2\pi f)|$, and $|w_\mathrm{T}(j2\pi f)|$, respectively. For the design of these weighting functions, the following recommendations given in (Skogestad & Postlethwaite, 2005) are taken into account:

- $|S(j2\pi f)|$ should be small within the control bandwidth to get good rejection of output disturbances Δn_y and good reference tracking, i.e., small control error.
- In favor of attenuation of sensor noise Δn_s (cf. Fig. 2) and robustness, the frequency response $|T(j2\pi f)|$ should be small at frequencies beyond the control bandwidth.
- $|C(j2\pi f)S(j2\pi f)|$ should be bounded to limit the control effort and oscillation amplitudes of the stopper rod due to output disturbances Δn_y.

Figure 5 also shows the chosen (inverse) weighting functions. Within the control bandwidth, $|w_\mathrm{S}(j2\pi f)|^{-1}$ is set equal to the sensitivity function achieved by the PI controller $C_\mathrm{PI}(s)$ defined in (8) for a typical (mean) plant gain $V_\mathrm{S} = 1.3\,\mathrm{m^2\,s^{-1}}$. For frequencies beyond the control bandwidth, $|w_\mathrm{S}(j2\pi f)|^{-1}$ is limited to a maximum value of 4 dB. These specifications are defined to ensure that the newly designed controller effectively suppresses unsteady bulging, cf. Section 2.3, while preserving the disturbance rejection performance typically achieved by the PI controller. In the same way, the inverse weighting function $|w_\mathrm{T}(j2\pi f)|^{-1}$ is set equal to the complementary sensitivity typically achieved by the PI controller. This specification aims to achieve the same level of robustness and attenuation of sensor noise Δn_s, cf. Fig. 2. Finally, $|w_\mathrm{CS}(j2\pi f)|^{-1}$ is set to 0 dB to limit stopper rod oscillations caused by output disturbances Δn_y and generally the control effort. Based on these specifications, the Matlab function `systune` solves the constrained optimization problem[3]

$$\min_{\mathbf{p}\in\mathbb{R}^{2m+1}} \max \overbrace{\left(\begin{bmatrix} ||w_S(s)\,S(s)||_\infty \\ ||w_{CS}(s)\,C(s)S(s)||_\infty \\ ||w_T(s)\,T(s)||_\infty \end{bmatrix} \right)}^{M(C(s))} \tag{21}$$

s.t. Stable basic mold level control loop (see Fig. 2)
with $C(s) = C_m(s)$ defined in (20) and
plant parameter uncertainties specified in (7),
maximum value of the gain K in (20),
$||w_{S_\mathrm{hard}}(s)\,S(s)||_\infty < 1$.

This formulation implies that the controller C_m of (fixed) order m is optimally tuned to minimize the objective function $M(C(s))$ across the entire range of plant parameter values. For this optimization, the gain K in (20) is set to its maximum value, which corresponds to a maximum mold area A and a minimum filling height h_t of the tundish (during normal casting). This accounts for the worst-case gain of $C(s)S(s)$ in the optimization. The objective function introduces soft constraints on $|S(j2\pi f)|$, $|CS(j2\pi f)|$, and $|T(j2\pi f)|$, where exceeding the related desired frequency responses $|w_\mathrm{S}(j2\pi f)|^{-1}$, $|w_\mathrm{CS}(j2\pi f)|^{-1}$, and $|w_\mathrm{T}(j2\pi f)|^{-1}$ at any frequency or for any combination of plant parameter values is penalized by a high objective function value $M(C(s)) > 1$. An objective function value below 1 indicates that $|w_\mathrm{S}(j2\pi f)|^{-1}$, $|w_\mathrm{CS}(j2\pi f)|^{-1}$, and $|w_\mathrm{T}(j2\pi f)|^{-1}$ are not exceeded, thereby ensuring that the specified control performance requirements are satisfied. However, to ensure robust stability of the overall mold level control loop and, thereby, effective suppression of unsteady bulging, maintaining $|S(j2\pi f)| < 4$ dB takes precedence over all other specifications. The Matlab function `systune` accepts additional hard constraints to enforce requirements like that. Hence, the hard constraint $\|w_{S_\mathrm{hard}}(s)S(s)\|_\infty < 1$ is included in the optimization, with the weighting function $w_{S_\mathrm{hard}}(s) = -4$ dB, cf. (21).

For the proposed controller design, robust stability of the overall mold level control loop is formally guaranteed only for constant plant parameters within the ranges specified in (7). Measurements at the considered industrial slab caster revealed that plant parameters vary significantly over time due to clogging or wear of the SEN or the stopper rod, or due to changes in casting conditions, e.g., casting speed, steel grade, or mold width. However, all these variations are much slower than the dynamics of the mold level control loop, i.e., its control bandwidth. According to (Khalil, 2002), stability can be still assumed for such slowly varying parameters. Although unclogging can lead to high mold level fluctuations and rapid changes in plant parameters, the measurements indicate that the magnitudes of these (temporal) parameter variations remain relatively small, as unclogging typically involves only partial deposit removal.

Values of the objective function $M(C(s))$ for controllers C_m of order $m = 1, 2, \ldots, 7$ are shown as blue circles in Fig. 12.

The case $m = 0$ (P controller) is not included in Fig. 12 because the desired slope of 40 dB/dec for $|w_\mathrm{S}(j2\pi f)|$ at low frequencies cannot be achieved with this controller and would result in $M(C(s)) \to \infty$. Increasing the controller order up to $m = 3$ yields a significant reduction of the objective function values, indicating improved control performance. For orders higher than $m = 3$, the improvements become negligible. This suggests that a controller of order $m = 3$ provides an optimal balance between control performance and complexity.

[3] The H_∞-norm of a stable scalar transfer function is equal to the peak value of its frequency response, see (Skogestad & Postlethwaite, 2005).

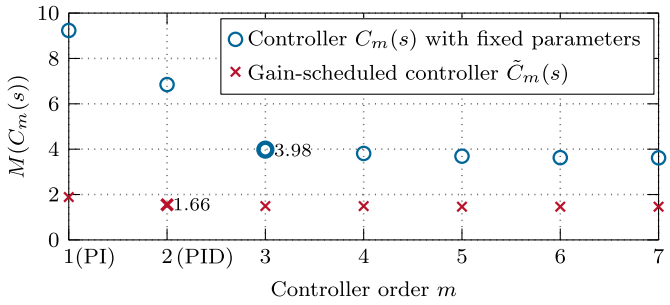

Fig. 12. Objective function value for the controller $C_m(s)$ with fixed parameters defined in (20) and for the gain-scheduled controller $\tilde{C}_m(s)$ defined in (22), evaluated for different controller orders m.

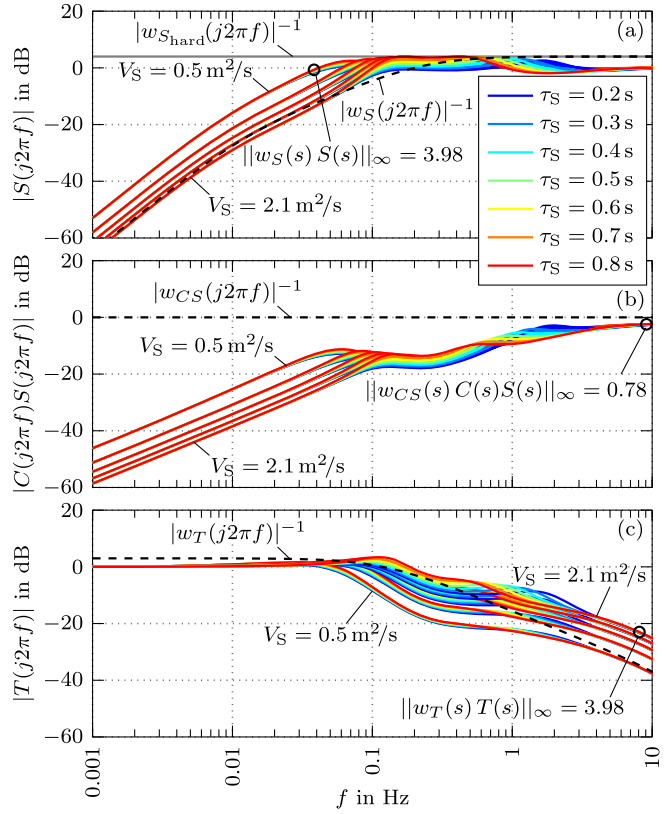

Fig. 13. Frequency responses of $S(s)$, $C(s)S(s)$, and $T(s)$ according to (9) for the optimized controller $C(s) = C_m(s)$ of order $m = 3$ defined in (20) and different values of the plant parameters V_S and τ_S.

Figure 13 shows the resulting frequency responses $|S(j2\pi f)|$, $|CS(j2\pi f)|$, and $|T(j2\pi f)|$ for the optimized controller $C(s) = C_3(s)$ and different plant parameter values. The magnitude and frequency values relevant for the total objective function value of $M(C(s)) = 3.98$ in Fig. 12 are also shown in Fig. 13, marked by ∘.

The frequency response $|C(j2\pi f)S(j2\pi f)|$ does not exceed the inverse
weighting function $|w_{CS}(j2\pi f)|^{-1}$ in Fig. 13(b).
Consequently, $||w_{CS}(s)\,C(s)S(s)||_\infty = 0.78$ is below 1. In contrast, $|S(j2\pi f)|$ and $|T(j2\pi f)|$ exceed their respective inverse weighting functions, and the corresponding H_∞-norms $||w_S(s)\,S(s)||_\infty$ and $||w_T(s)\,T(s)||_\infty$ are both 3.98. This means that the inverse weighting functions $|w_S(j2\pi f)|^{-1}$ and $|w_T(j2\pi f)|^{-1}$ are exceeded by up to approximately 12 dB. Figure 13(a) shows that the sensitivity peaks are all below 4 dB, as enforced by the hard constraint $\|w_{S_{\text{hard}}}(s)S(s)\|_\infty < 1$ in (21). Therefore, the optimized controller $C_3(s)$ can effectively suppress unsteady bulging, cf. Section 2.3. However, the previously used PI controller $C_{\text{PI}}(s)$ defined in (8) achieves lower sensitivity function values within the control bandwidth, see Fig. 5(a) in comparison to Fig. 13(a), indicating a higher control performance in terms of disturbance rejection. Clearly, lower values of the sensitivity function within the control bandwidth achieved by the PI controller come at the risk of high sensitivity peaks, which may destabilize the overall mold level control loop (trigger unsteady bulging) and amplify other disturbances in the corresponding frequency ranges. While the control performance of the optimized controller $C_3(s)$ remains limited, it guarantees a stable overall mold level control loop and still surpasses the control performance of the PI controller with reduced overall control gain, see Fig. 10 in comparison to Fig. 13(a).

This section demonstrated that suppressing unsteady bulging by a feedback controller with fixed parameters entails a reduction of the control performance regarding disturbance rejection compared to the previously used PI controller (8). This performance limitation stems from significant variations in the plant parameters specified in (7). The optimized controller C_m was designed to handle the entire range of plant parameter values while maintaining the stability of the overall mold level control loop, even for the worst-case combination of the possible plant parameter values. To overcome the performance limitations of controllers with fixed parameters, the following section introduces a gain-scheduled controller that dynamically adapts its parameters to variations in the plant parameters.

3.2. Gain-scheduled controller

As already mentioned in the previous section, significant variations in the plant parameters V_S and τ_S typically evolve at a rate significantly slower than the control bandwidth. Gain scheduling can thus be an effective approach for enhancing the control performance by adjusting the controller parameters in response to changes in the plant parameters, see, e.g., (Khalil, 2002; Rugh & Shamma, 2000; Shamma & Athans, 1992; Wang & Sundararajan, 1995). This requires that the parameters V_S and τ_S are estimated online, i.e., in real-time, e.g., in the same way as described in Section 2.1 using (6). To facilitate this online estimation, an additional harmonic oscillation Δu^e with a specific frequency f_e is continuously commanded to the stopper rod (see Fig. 2), inducing small mold level fluctuations. The amplitude of these fluctuations is selected small enough not to affect the product quality, but high enough to ensure a sufficient signal-to-noise ratio for accurate online parameter estimation, i.e., $V_S^e \approx V_S$ and $\tau_S^e \approx \tau_S$. Tests conducted on the real plant revealed a high accuracy of this online parameter estimation. Remaining minor inaccuracies can be tolerated, as they are accounted for by the robustness of the controller. Therefore, for the sake of simplicity, $V_S^e = V_S$ and $\tau_S^e = \tau_S$ are assumed in the following.

The estimated parameter values are then used to adapt the controller transfer function (20) in the form

$$\tilde{C}_m(s, V_S, \tau_S) = \underbrace{A\sqrt{\frac{h_t^0}{h_t}}\frac{1}{V_S}}_{\tilde{K}(V_S)} \cdot \underbrace{\frac{b_m(\tau_S)s^m + b_{m-1}(\tau_S)s^{m-1} + \ldots + b_1(\tau_S)s + b_0(\tau_S)}{s^m + a_{m-1}(\tau_S)s^{m-1} + \ldots + a_1(\tau_S)s + a_0(\tau_S)}}_{\tilde{C}_m^0(s,\tau_S)}. \quad (22)$$

In contrast to (20), $\tilde{K}$ is additionally adapted based on the estimated gain V_S to eliminate the influence of V_S on the open-loop transfer function $G(s)C(s)$ and, consequently, on the control performance. The remaining controller parameters $\tilde{\mathbf{p}} = [a_0, a_1, \ldots, a_{m-1}, b_0, b_1, \ldots, b_m]^T$ in (22) are thus adapted based on the dead time τ_S only. The optimal gain schedule is determined by sequentially solving the constrained optimization

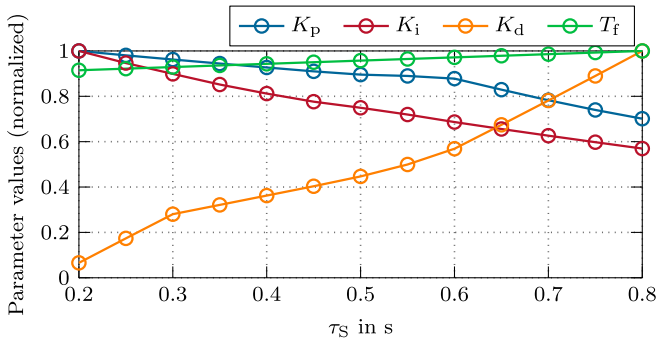

Fig. 14. Optimal gain schedule for the PID controller (24). The parameter values are normalized with respect to their maximum values.

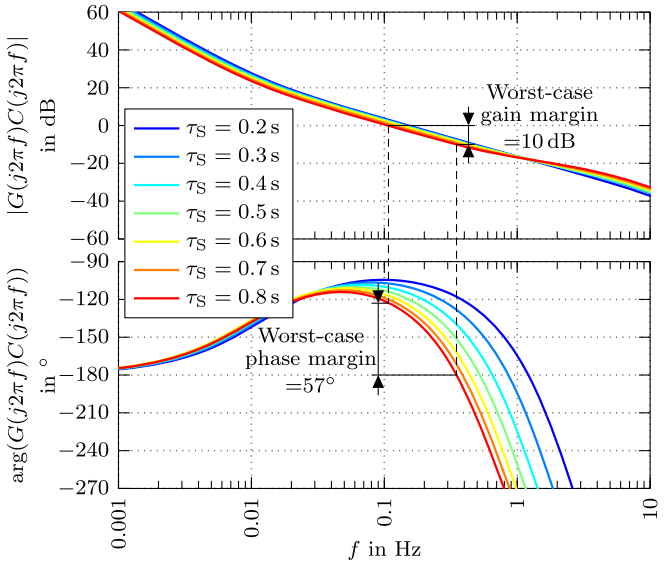

Fig. 15. Frequency response of the open basic mold level control loop $G(s)C(s)$, cf. Fig. 2, for the gain-scheduled PID controller $C(s) = \tilde{C}_\mathrm{PID}(s, V_\mathrm{S}, \tau_\mathrm{S})$ defined in (24) and different values of the dead time τ_S. The dependence on V_S is canceled out by $\tilde{K}(V_\mathrm{S})$ in (24).

problem

$$\min_{\tilde{\mathbf{p}} \in \mathbb{R}^{2m+1}} \overbrace{\max\left(\begin{bmatrix} ||w_S(s)\,S(s)||_\infty \\ ||w_{CS}(s)\,C(s)S(s)||_\infty \\ ||w_T(s)\,T(s)||_\infty \end{bmatrix} \right)}^{M(C(s))} \tag{23}$$

s.t. Stable basic mold level control loop (see Fig. 2)
with $C(s) = \tilde{C}_m(s, V_\mathrm{S}, \tau_\mathrm{S})$ according to (22),
maximum value of the gain $\tilde{K}$ in (22),
$\tau_\mathrm{S} \in \tau_\mathrm{S}^{\mathrm{design}}$,
$||w_{S_\mathrm{hard}}(s)\,S(s)||_\infty < 1$

for different dead times τ_S selected from the set $\tau_\mathrm{S}^{\mathrm{design}} = [0.2, 0.25, 0.3, \ldots, 0.8]$s, see also (7). Similar to (21), the optimization is performed for maximum gain $\tilde{K}$, which occurs for maximum mold area A, minimum filling height h_t of the tundish, and minimum plant gain V_S, cf. (22). In this way, the worst-case gain of $C(s)S(s)$ is considered in the optimization. Figure 12 also shows the objective function values for $\tilde{C}_m(s, V_\mathrm{S}, \tau_\mathrm{S})$ of orders $m = 1, 2, \ldots, 7$, defined in (22). It demonstrates that the gain-scheduled controller $\tilde{C}_m(s, V_\mathrm{S}, \tau_\mathrm{S})$ significantly reduces the objective function values and improves control performance compared to the controller $C_m(s)$ with fixed

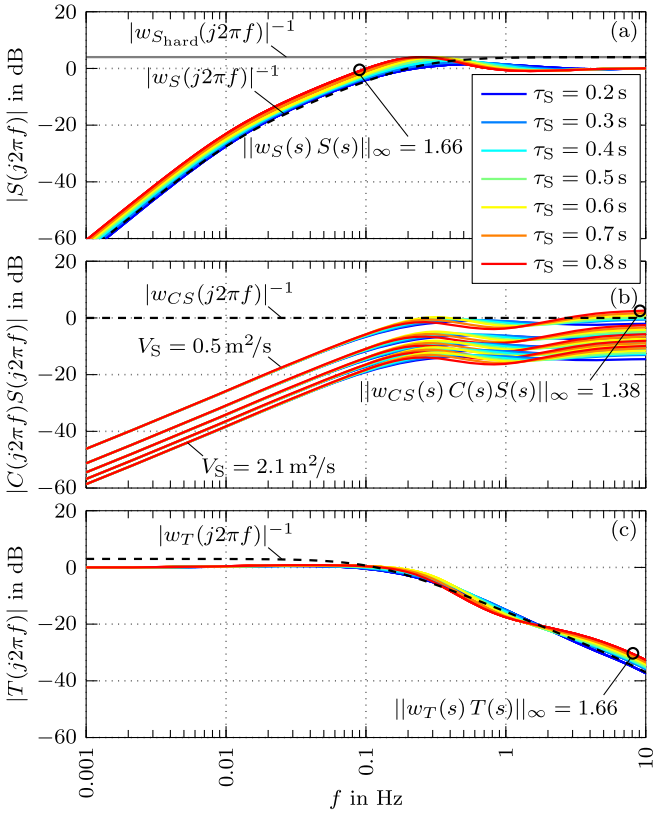

Fig. 16. Frequency responses of $S(s)$, $C(s)S(s)$, and $T(s)$ according to (9) for the gain-scheduled PID controller $C(s) = \tilde{C}_\mathrm{PID}(s, V_\mathrm{S}, \tau_\mathrm{S})$ defined in (24) and different values of the plant parameters V_S and τ_S.

parameters defined in (20). Furthermore, Fig. 12 indicates that the low objective function values are already achieved for a controller of order $m = 2$. For gain-scheduled controllers of order $m > 2$, only marginal performance improvements are observed. Consequently, the gain-scheduled controller $\tilde{C}_m(s, V_\mathrm{S}, \tau_\mathrm{S})$ of order $m = 2$ is examined in more detail in the following analysis. To simplify implementation at the real plant, the controller of order $m = 2$ is restricted to a PID controller by forcing one pole to the value $s = 0$ (ideal integrator). This is done by setting $a_0 = 0$ in (22). This restriction does not compromise the achievable performance because the optimal objective function value $M(C_2(s)) = 1.66$ in Fig. 12 is still attained. The gain-scheduled PID controller can be expressed in the (parallel) form

$$\tilde{C}_\mathrm{PID}(s, V_\mathrm{S}, \tau_\mathrm{S}) = \underbrace{A\sqrt{\frac{h_\mathrm{t}^0}{h_\mathrm{t}}}\frac{1}{V_\mathrm{S}}}_{\tilde{K}(V_\mathrm{S})} \underbrace{\left(K_\mathrm{p}(\tau_\mathrm{S}) + \frac{K_\mathrm{i}(\tau_\mathrm{S})}{s} + \frac{sK_\mathrm{d}(\tau_\mathrm{S})}{1 + sT_\mathrm{f}(\tau_\mathrm{S})} \right)}_{\tilde{C}^0_\mathrm{PID}(s, \tau_\mathrm{S})}, \tag{24}$$

with the parameters

$$\tilde{\mathbf{p}} = \begin{bmatrix} K_\mathrm{p} & K_\mathrm{i} & K_\mathrm{d} & T_\mathrm{f} \end{bmatrix}^\mathrm{T}. \tag{25}$$

K_p, K_i, and K_d denote the gains of the proportional, integral, and derivative parts of the PID controller, respectively. Solving the optimization problem (23) with $C(s) = \tilde{C}_\mathrm{PID}(s, V_\mathrm{S}, \tau_\mathrm{S})$ defined in (24) gives the optimal gain schedule shown in Fig. 14. The proposed gain-scheduled PID controller decreases its proportional and integral gain and increases its derivative gain as the dead time increases. Figure 15 shows the frequency response of the open-loop transfer function $G(s)C(s)$ for the gain-scheduled PID controller $C(s) = \tilde{C}_\mathrm{PID}(s, V_\mathrm{S}, \tau_\mathrm{S})$. The open loop no longer depends on the plant gain V_S when using the gain-scheduled PID controller instead of the PI controller (8) (with fixed parameters), cf. Fig. 6. This is because the dependence of the open loop $G(s)C(s)$ on V_S is can-

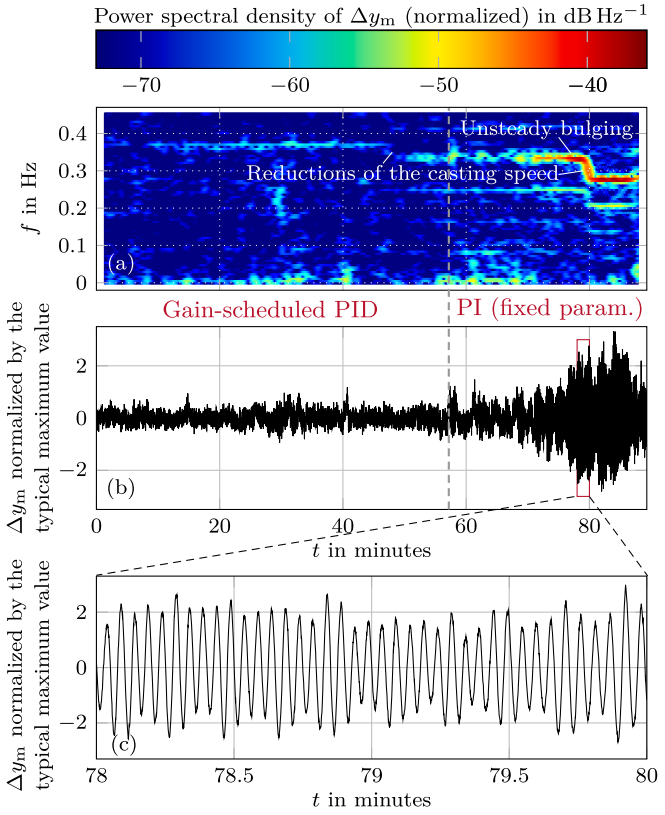

Fig. 17. Comparison between the PI controller (previously used controller with fixed parameters) defined in (8) and the gain-scheduled PID controller defined in (24) during unsteady bulging, measured on an industrial slab caster, (a) spectrogram of the mold level fluctuations, (b) mold level fluctuations, (c) mold level fluctuations in a zoomed time interval with high unsteady bulging.

celed out by $\tilde{K}(V_S)$ in (24) (assuming exact estimation, i.e., $V_S^e = V_S$). Furthermore, Fig. 15 demonstrates that adapting the controller parameters according to Fig. 14 guarantees phase and gain margins of at least 57° and 10 dB, respectively (compared to 10° and 1 dB for the PI controller (8) in Fig. 6). This also indicates a high robustness of the basic mold level control loop with respect to errors in the estimation of the plant parameters V_S and τ_S.

The frequency responses of $S(s)$, $T(s)$, and $C(s)S(s)$ for the gain-scheduled PID controller $C(s) = \tilde{C}_{PID}(s, V_S, \tau_S)$ are shown in Fig. 16. The objective function value $M(\tilde{C}_{PID}(s, V_S, \tau_S)) = 1.66$ (see Fig. 12) is attained by both $||w_S(s)\,S(s)||_\infty$ and $||w_T(s)\,T(s)||_\infty$. Because the open-loop transfer function $G(s)C(s)$ does not depend on the plant gain V_S for $C(s) = \tilde{C}_{PID}(s, V_S, \tau_S)$, it follows that the sensitivity function $S(s)$ and complementary sensitivity function $T(s)$ are also independent of it, cf. (9). This implies that the impact of plant parameter variations on the control performance is significantly reduced when using the gain-scheduled PID controller (24) instead of a fixed-parameter controller ((8) or (20)). This can also be inferred from a comparison of Figs. 16, 13, and 5. Furthermore, the sensitivity peaks in Fig. 16(a) are all below 4 dB, which ensures effective suppression of unsteady bulging. For low dead times, the desired curves $|w_S(j2\pi f)|^{-1}$, $|w_{CS}(j2\pi f)|^{-1}$, and $|w_T(j2\pi f)|^{-1}$ are (almost) not exceeded, and the desired control performance is therefore achieved. Even for high dead times, the desired frequency responses are only slightly exceeded. Hence, the proposed gain-scheduled PID controller effectively suppresses unsteady bulging and, at the same time, achieves a level of disturbance rejection performance comparable to that of the previously used PI controller.

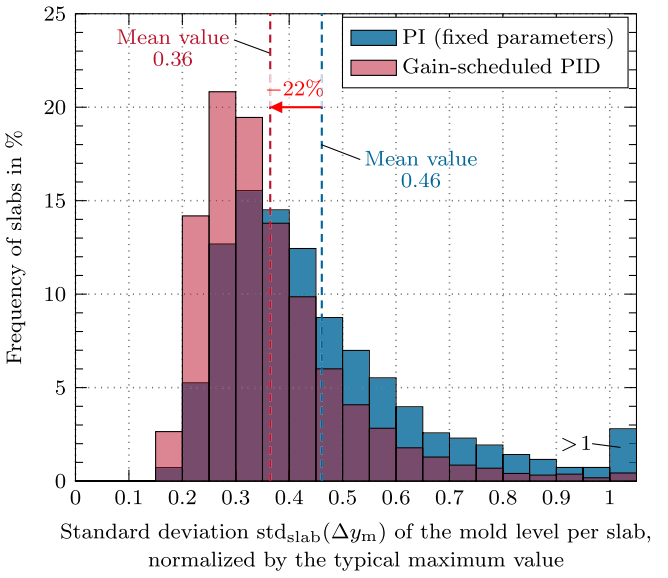

Fig. 18. Comparison of mold level fluctuations during the production of slabs using the PI controller (10015 slabs) defined in (8) and the gain-scheduled PID controller (7860 slabs) defined in (24).

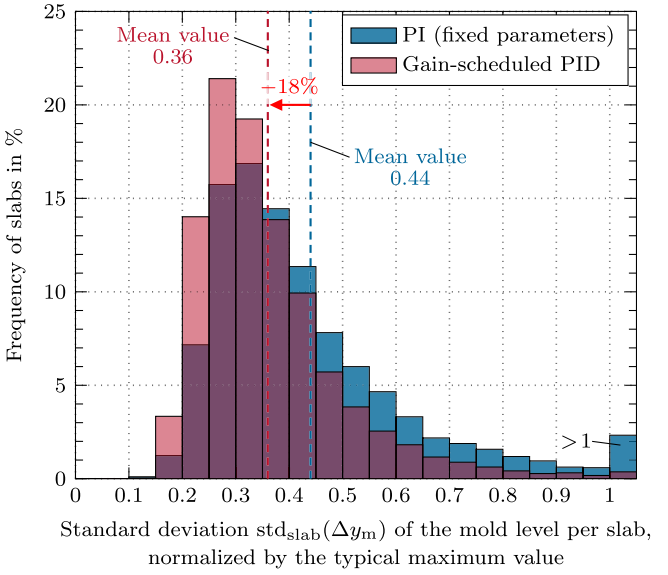

Fig. 19. Overall result across all slab casters at voestalpine Stahl GmbH, comparing mold level fluctuations for 12372 slabs cast using the PI controller defined in (8) and 9732 slabs using the gain-scheduled PID controller defined in (24).

4. Validation of the gain-scheduled PID controller on industrial slab casters

The gain-scheduled PID controller and the online estimation of the plant parameters V_S and τ_S described in Section 3.2 were implemented on an industrial continuous slab caster at voestalpine Stahl GmbH. For that implementation, the gain schedule for the design points $\tau_S^{design} = [0.2, 0.25, 0.3, \ldots, 0.8]$s, shown in Fig. 14, is stored in a lookup table. Values between these points are computed by linear interpolation. The parameters V_S and τ_S are continuously estimated and used for online (real-time) adaptation of the controller (24). The gain-scheduled PID controller was tested on an industrial continuous slab caster by alternately applying the PI controller (8) (previously used controller with

fixed parameters) and the gain-scheduled PID controller (24) during slab casting. Figure 17 shows an example of these tests. During the first 57 minutes, the gain-scheduled PID controller is active. Unsteady bulging is successfully suppressed, and the remaining mold level fluctuations are relatively low. For $t > 57$ minutes, the PI controller is active, leading to increased mold level fluctuations and the onset of unsteady bulging with rapidly growing amplitudes, i.e., an instability of the overall mold level control loop.

These tests and validations were carried out over several months, covering a total of 17875 slabs (10015 slabs were cast using the PI controller with fixed parameters and 7860 slabs using the gain-scheduled PID controller). The obtained measurement results indicate a reduction of mold level fluctuations across all operating conditions (i.e., casting speeds, steel grades, mold widths, etc.). The histogram in Fig. 18 summarizes these test results. It presents the relative frequency distribution of the slabs grouped by specific ranges of the mold level standard deviation $\mathrm{std}_{\mathrm{slab}}(\Delta y_{\mathrm{m}})$ (normalized), measured during their production. The number of slabs with normalized standard deviation greater than 0.35 is significantly reduced by the gain-scheduled PID controller, resulting in 22 % reduction of the mean value of the standard deviation. This improvement is primarily attributed to the suppression of high mold level fluctuations caused by unsteady bulging. In addition, the reduction of sensitivity peaks, see Fig. 16(a) compared to Fig. 5(a), leads to significantly lower mold level fluctuations in the corresponding frequency range, which can be induced, e.g., by turbulent steel flow patterns in the SEN and the mold. As a result, the number of slabs requiring postprocessing and the associated high additional costs are significantly reduced.

Following this success, tests of the gain-scheduled PID controller were extended to all continuous slab casters at voestalpine Stahl GmbH, where an additional 4229 slabs were cast (2357 using the PI controller with fixed parameters and 1872 slabs using the gain-scheduled PID controller). Figure 19 shows the overall result across all slab casters, which is consistent with the result shown in Fig. 18. Due to the significant reduction in mold level fluctuations across all casters, the previously used PI controller was replaced by the gain-scheduled PID controller at each caster. The new controller has demonstrated stable operation and excellent performance for over a year to date.

5. Conclusions

This paper presented a robust mold level controller design for continuous slab casters. Its main purpose is to suppress unsteady bulging. Landauer et al. (2024) showed that unsteady bulging is linked to an instability of the overall mold level control loop, including the basic mold level control loop and an internal feedback loop associated with unsteady bulging, the so-called bulging loop. In the literature, unsteady bulging is typically ignored or modeled as an exogenous harmonic disturbance with constant amplitude for the design of the mold level controller. Consequently, disturbance-feedforward concepts in addition to the basic mold level controller are often proposed to actively suppress mold level fluctuations caused by unsteady bulging. The drawback of these approaches is that even a small model-plant mismatch can significantly degrade control performance. In contrast to the existing literature, the present paper explicitly accounts for the bulging loop and its destabilizing effect by incorporating a control-oriented unsteady bulging model in the controller design.

It has been shown that reliable suppression of unsteady bulging does not necessarily require active damping, as introduced by an additional disturbance-feedforward controller, but can be achieved through a tailored design of the mold level controller that ensures stability of the overall mold level control loop. Specifically, the peak of the sensitivity function of the basic mold level control loop (sensitivity peak) has to be kept below a certain maximum value. This is a challenging design problem due to high variations in plant parameters resulting from clogging and wear of the stopper rod and the SEN, as well as changes in operating conditions. The problem is solved by a robust controller design using the Matlab function `systune`. This function optimally tunes the parameters of a controller to maintain robust stability of the overall mold level control loop, i.e., stability across the entire range of operating conditions, thereby suppressing unsteady bulging. Specifically, the development of a robust controller with fixed parameters and a robust gain-scheduled controller was presented. Both controllers were shown to reliably suppress unsteady bulging, in contrast to the previously used PI controller. However, achieving this with the fixed-parameter controller entails a considerable limitation in control performance. In contrast, the proposed gain-scheduled controller ensures robust stability while delivering high control performance by dynamically adjusting its gains in response to variations in plant parameters. For this purpose, a method for online estimation of the plant parameters was developed. The gain-scheduled controller was successfully tested on the industrial continuous slab casters at voestalpine Stahl GmbH, where it has since been deployed and demonstrates excellent performance.

CRediT authorship contribution statement

Julian Landauer: Writing – original draft, Validation, Software, Methodology, Investigation, Formal analysis; **Paul Dollhäubl:** Validation, Software, Resources, Data curation; **Stefan Fuchshumer:** Writing – review & editing, Validation, Supervision, Resources, Data curation; **Wilhelm Posch:** Validation, Resources, Data curation; **Andreas Kugi:** Writing – review & editing, Supervision, Resources, Funding acquisition; **Andreas Steinboeck:** Writing – review & editing, Supervision, Resources, Project administration, Funding acquisition, Formal analysis, Conceptualization.

Declaration of competing interest

The authors declare that they have no known competing financial interests or personal relationships that could have appeared to influence the work reported in this paper.

Acknowledgments

The financial support by the Austrian Federal Ministry of Economy, Energy and Tourism, the National Foundation for Research, Technology and Development, the Christian Doppler Research Association, and voestalpine Stahl GmbH is gratefully acknowledged. The authors acknowledge TU Wien Bibliothek for financial support through its Open Access Funding Programme.

References

Apkarian, P., Dao, M. N., & Noll, D. (2015). Parametric robust structured control design. *IEEE Transactions on Automatic Control*, *60*(7), 1857–1869.

Apkarian, P., Gahinet, P., & Buhr, C. (2014). Multi-model, multi-objective tuning of fixed-structure controllers. In *2014 European control conference (ECC)* (pp. 856–861).

Apkarian, P., & Noll, D. (2006). Nonsmooth H_∞ synthesis. *IEEE Transactions on Automatic Control*, *51*(1), 71–86.

Apkarian, P., & Noll, D. (2007). Nonsmooth optimization for multiband frequency domain control design. *Automatica*, *43*(4), 724–731.

Asano, K., Kaji, T., Aoki, H., Ibaraki, M., & Moriwaki, S., et al. (1996). Robust molten steel level control for continuous casting. In *Proceedings of 35th IEEE conference on decision and control* (pp. 1245–1250). (*vol. 2*).

Azizi, G., Thomas, B. G., & Asle Zaeem, M., et al. (2020). Review of peritectic solidification mechanisms and effects in steel casting. *Metallurgical and Materials Transactions B*, *51*(5), 1875–1903.

Bai, H., & Thomas, B. G. (2001). Effects of clogging, argon injection, and continuous casting conditions on flow and air aspiration in submerged entry nozzles. *Metallurgical and Materials Transactions B*, *32*(4), 707–722.

Craig, I. K., Camisani-Calzolari, F. R., & Pistorius, P. C. (2001). A contemplative stance on the automation of continuous casting in steel processing. *Control Engineering Practice*, *9*(9), 1013–1020.

Cukierski, K., & Thomas, B. G. (2008). Flow control with local electromagnetic braking in continuous casting of steel slabs. *Metallurgical and Materials Transactions B*, *39*(1), 94–107.

De Keyser, R. M. C. (1997). Improved mould-level control in a continuous steel casting line. *Control Engineering Practice*, *5*(2), 231–237.

Feng, Y., Wu, M., Chen, X., Chen, L., & Du, S. (2020). A fuzzy PID controller with nonlinear compensation term for mold level of continuous casting process. *Information Sciences*, *539*, 487–503.

Furtmueller, C., Colaneri, P., & del Re, L., et al. (2012). Adaptive robust stabilization of continuous casting. *Automatica*, *48*(1), 225–232.

Furtmueller, C., & del Re, L. (2008). Control issues in continuous casting of steel. *IFAC Proceedings Volumes*, *41*(2), 700–705.

González-Yero, G., Mendoza, M. R., & Albertos, P. (2018). Robust non linear adaptive mould level control for steel continuous casting. *IFAC-PapersOnLine*, *51*, 164–170.

González-Yero, G., Ramírez Leyva, R., Ramírez Mendoza, M., Albertos, P., Crespo-Lorente, A., & Reyes Alonso, J. M. (2021). Neuro fuzzy system for compensating slow disturbances in adaptive mold level control. *Metals*, *11*, 1–20.

Hirschmanner, M., Mörwald, K., & Fröhlich, C., et al. (2011). Next generation mold level control: Development of LevCon 2.0. *Materials and Manufacturing Processes*, *26*(1), 169–174.

Iijima, Y., & Mizuno, H. (2007). Gain-scheduled H-infinity control of molten steel level in the mold of a continuous steel caster. *IFAC Proceedings Volumes*, *40*(11), 213–218.

Jabri, K. (2010). Etude et amélioration des performances et de la robustesse des lois de commande de procédés sidérurgiques Application à la régulation de niveau en coulée continue. Ph.D. thesis. Université Paris Sud - Paris XI.

Jabri, K., Bele, B., Mouchette, A., Godoy, E., & Dimur, D., et al. (2008). Disturbances estimation for mold level control in the continuous casting process. In *Proceedings of the international conference on informatics in control, automation and robotics* (pp. 119–124). (*vol. SPSMC*).

Jabri, K., Godoy, E., Dumur, D., Mouchette, A., & Bèle, B. (2010). Robust adaptive control of the mold level in the continuous casting process using multiple models. In *Proceedings of the American control conference* (pp. 6101–6108).

Jabri, K., Godoy, E., Dumur, D., Mouchette, A., & Bèle, B., et al. (2011). Cancellation of bulging effect on mould level in continuous casting: Experimental validation. *Journal of Process Control*, *21*(2), 271–278.

Khalil, H. K. (2002). Nonlinear systems. (3rd ed.). Upper Saddle River, New York: Prentice Hall.

Kim, M., Moon, S., Na, C., Lee, D., Kueon, Y., & Lee, J. S., et al. (2011). Control of mold level in continuous casting based on a disturbance observer. *Journal of Process Control*, *21*(7), 1022–1029.

Kitada, H., Kondo, O., Kusachi, H., & Sasame, K., et al. (1998). H_∞ control of molten steel level in continuous caster. *IEEE Transactions on Control Systems Technology*, *6*(2), 200–207.

Kong, F., & de Keyser, R. (1993). Identification and control of the mould level in a continuous casting machine. In *Proceedings of the IEEE international conference on control and applications* (pp. 53–58). (*vol. 1*).

Kozlowski, P. F., Thomas, B. G., Azzi, J. A., & Wang, H., et al. (1992). Simple constitutive equations for steel at high temperature. *Metallurgical and Materials Transactions A*, *23*(3), 903–918.

Kurokawa, T., Kondo, T., Mita, T., Liu, K., & Sampei, M. (1993). Development of mold level control in continuous casting by H-infinity control theory. In *Proceedings of the IEEE international conference on control and applications* (pp. 865–871).

Lamant, J. Y., Larrecq, M., Birat, J. P., Hensgen, J. L., Weber, J. D., & Dhuyvetter, J. C., et al. (1985). Study of slab bulging in continuous caster. In *Proceedings of the international conference on continuous casting* (pp. 37.1–37.8).

Lamant, J. Y., Larrecq, M., Mouchette, A., Codur, Y., Gancarz, J., & Leclercq, A., et al. (1990). Advanced control of mold operation and improved slab surface quality on sollac continuous casters. In *Proceedings of the international iron and steel Congress.* (pp. 317–324). (*vol. 3*).

Landauer, J., Marko, L., Kugi, A., & Steinboeck, A., et al. (2024). Mathematical modeling and system analysis for preventing unsteady bulging in continuous slab casting machines. *Journal of Process Control*, *139*, 103232.

Lee, J. D., & Yim, C. H. (2000). The mechanism of unsteady bulging and its analysis with the finite element method for continuously cast steel. *ISIJ International*, *40*(8), 765–770.

Lee, S., Lee, Y., Park, B., & Lee, C. (2024). Structural optimization of scarfing machine with acceleration profile and multi-objective genetic algorithm approach. *Machines*, *12*(6), 398.

Lei, H., Liu, J., Tang, G., Zhang, H., Jiang, Z., & Lv, P., et al. (2023). Deep insight into mold level fluctuation during casting different steel grades. *JOM Journal of the Minerals Metals and Materials Society*, *75*(3), 914–919.

Murakami, T., Kawamoto, M., Kitada, H., & Hanao, M. (2004). New technology to prevent periodical level fluctuation in continuous casting (development of variable pitch segment). *Kang T'ieh/Iron and Steel*, *39*, 338–341.

Rugh, W. J., & Shamma, J. S. (2000). Research on gain scheduling. *Automatica*, *36*(10), 1401–1425.

Saleem, A., Underhill, P. R., Chataway, D., Gerritsen, T., Sadri, A., & Krause, T. W., et al. (2020). Electromagnetic measurement of molten metal level in pyrometallurgical furnaces. *IEEE Transactions on Instrumentation and Measurement*, *69*(6), 3118–3125.

Schuurmans, J., Kamperman, A., Middel, B., & van den Bosch, P. (2005). Robust mould level control. In *Proceedings of the American control conference, IEEE* (pp. 2040–2045).

Shamma, J. S., & Athans, M. (1992). Gain scheduling: Potential hazards and possible remedies. *IEEE Control Systems Magazine*, *12*(3), 101–107.

Skogestad, S., & Postlethwaite, I. (2005). Multivariable feedback control: Analysis and design. New York: John Wiley & Sons.

Tacke, K. H. (2014). Irregular and fluctuating phenomena in continuous casting. In *Proceedings of the European continuous casting conference and symposium in numerical & physical modeling* (pp. 23–26).

Wang, J., & Sundararajan, N. (1995). A nonlinear flight controller design for aircraft. *Control Engineering Practice*, *3*(6), 813–825.

Xia, G., Bernhard, C., Ilie, S., & Fuerst, C., et al. (2011). A study about the influence of carbon content in the steel on the casting behavior. *Steel Research International*, *81*(12), 1–7.

Yoon, U.-S., Bang, I.-W., Rhee, J. H., Kim, S.-Y., Lee, J.-D., & Oh, K. H., et al. (2002). Analysis of mold level hunching by unsteady bulging during thin slab casting. *ISIJ International*, *42*(10), 1103–1111.

You, B., Kim, M., Lee, D., Lee, J., & Lee, J. S. (2011). Iterative learning control of molten steel level in a continuous casting process. *Control Engineering Practice*, *19*(3), 234–242.

Zhang, K.-T., Liu, J.-H., & Cui, H. (2020). Effect of flow field on surface slag entrainment and inclusion adsorption in a continuous casting mold. *Steel Research International*, *91*(2), 1900437.

Zhang, X., & Ji, Z. (2014). Research of mold level control algorithm based on hybrid control strategy. In *Proceedings of the 6th international conference on intelligent human-machine systems and cybernetics* (pp. 130–133).